Different Impacts of Various El Niño Events on the Indian Ocean Dipole

Xin Wang [1, 2 & 3]

Chunzai Wang [2]

[1] Cooperative Institute for Marine and Atmospheric Studies

University of Miami

Miami, Florida

[2] NOAA Atlantic Oceanographic and Meteorological Laboratory

Miami, Florida

[3] State Key Laboratory of Tropical Oceanography, South China Sea Institute of Oceanology

Chinese Academy of Sciences, Guangzhou, China

Revised to *Climate Dynamics*

January 2013

Corresponding author address: Dr. Chunzai Wang, Physical Oceanography Division, NOAA/Atlantic Oceanographic and Meteorological Laboratory, 4301 Rickenbacker Causeway, Miami, FL 33149, USA.
E-mail: chunzai.wang@noaa.gov.

Abstract

Our early work (Wang and Wang 2013) separates El Niño Modoki events into El Niño Modoki I and II because they show different impacts on rainfall in southern China and typhoon landfall activity. The warm SST anomalies originate in the equatorial central Pacific and subtropical northeastern Pacific for El Niño Modoki I and II, respectively. El Niño Modoki I features a symmetric SST anomaly distribution about the equator with the maximum warming in the equatorial central Pacific, whereas El Niño Modoki II shows an asymmetric distribution with the warm SST anomalies extending from the northeastern Pacific to the equatorial central Pacific. The present paper investigates the influence of the various groups of El Niño events on the Indian Ocean Dipole (IOD). Similar to canonical El Niño, El Niño Modoki I is associated with a weakening of the Walker circulation in the Indo-Pacific region which decreases precipitation in the eastern tropical Indian Ocean and maritime continent and thus results in the surface easterly wind anomalies off Java-Sumatra. Under the Bjerknes feedback, the easterly wind anomalies induce cold SST anomalies off Java- Sumatra, and thus a positive IOD tends to occur in the Indian Ocean during canonical El Niño and El Niño Modoki I. However, El Niño Modoki II has an opposite impact on the Walker circulation, resulting in more precipitation and surface westerly wind anomalies off Java-Sumatra. Thus, El Niño Modoki II is favorable for the onset and development of a negative IOD on the frame of the Bjerknes feedback.

1. Introduction

The Indian Ocean Dipole (IOD), a coupled ocean-atmosphere phenomenon in the tropical Indian Ocean, has been extensively studied in the recent decades (e.g., Saji et al. 1999; Webster et al. 1999; Baquero-Bernal et al. 2002; Saji and Yamagata 2003; Meyers et al. 2007; Luo et al. 2008). The positive IOD features a zonal gradient of tropical sea surface temperature (SST) with cooling off Java-Sumatra and warming in the western tropical Indian Ocean. The IOD usually begins to develop in boreal summer, peaks in fall, and decays rapidly in winter, which is seasonally modulated by the Asian monsoon wind and the Indian Ocean mean states (Saji et al. 1999; Xiang et al. 2011). A number of studies have documented that the changes in the IOD exert great impacts on climate variability in South Asia, East Asia, Australia, and other regions (e.g., Ashok et al. 2003, 2004; Saji and Yamagata 2003; Li et al. 2006; Wang et al. 2006; Yuan et al. 2008; Cai et al. 2009).

It is shown that some IOD events in the 20th century can co-occur with El Niño-Southern Oscillation (ENSO), while some are independent of ENSO (Saji and Yamagata 2003; Meyers et al 2007). The ENSO-induced IOD events are forced by a zonal shift in the descending branch of the Walker circulation over the eastern Indian Ocean (Ueda and Matsumoto 2001; Hastenrath 2002; Baquero-Bernal et al. 2002; Krishnamurthy and Kirtman 2003; Fischer et al. 2005; Annamalai et al. 2003; Vecchi and Soden 2007). Besides ENSO, other external drivers can also induce the IOD occurrence, such as the Southern Annular Mode (Lau and Nath 2004) and monsoon (Fischer et al. 2005). Some IOD events (such as 1961, 1967, 1997 and 2007) may be originated from the internal physical processes in the Indian Ocean with regard to the strong easterly wind disturbance (e.g., Saji et al. 1999; Vinayachandran et al. 1999; Yamagata et al. 2003; Behera et al. 2006; Luo et al. 2008; Schott et al. 2009).

Recently, the ENSO research community has focused on the eastern Pacific warm event (or canonical El Niño) and the central Pacific warm event. The central Pacific El Niño (Yu and Kao 2007) is also referred to as Dateline El Niño (Larkin and Harrison 2005), El Niño Modoki (Ashok et al. 2007), or warm pool El Niño (Kug et al. 2009). Wang et al. (2013) provide an ENSO overview including the two types of ENSO events and their different climate impacts and mechanisms. In this study, the name of El Niño Modoki is used. El Niño Modoki is characterized by the maximum SST anomalies locating in the central tropical Pacific instead of the eastern tropical Pacific for canonical or conventional El Niño. The impacts of El Niño Modoki on the tropical and midlatitude climate are distinct from these of canonical El Niño because the intensity and location of their associated SST-induced heating are different (e.g., Larkin and Harrison 2005; Ashok et al. 2007; Weng et al. 2007; Feng et al. 2011; Yuan and Yang 2012; Kim et al. 2012).

The relationships between El Niño Modoki and the IOD are not completely known yet. Ashok et al. (2007) suggested that El Niño Modoki is weakly related to the IOD during 1958-2005. During summer of the 2004 El Niño Modoki event, there is no significant IOD pattern (Ashok et al. 2009). These results seem to illustrate a weak relationship between El Niño Modoki and the IOD. However, Luo et al. (2008, 2010) suggested that El Niño Modoki and the positive IOD could occur simultaneously and influence each other. The observed results indicate that the western and central tropical Pacific warming is a precursor condition for the positive IOD occurrence (Annamalai et al. 2003). The positive IOD events can even be predicted 1-2 seasons ahead by fully coupled model with the central tropical Pacific warming (Song et al. 2007, 2008).

Based on the opposite influence on rainfall in southern China and typhoon landfall activity during boreal fall, Wang and Wang (2013) classify and name El Niño Modoki I and II. The identified El Niño Modoki I and II events also show different origins and patterns of SST anomalies in the tropical Pacific. The warm SST anomalies originate in the equatorial central Pacific and subtropical northeastern Pacific for El Niño Modoki I and II, respectively. El Niño Modoki I shows a symmetric SST anomaly distribution about the equator with the maximum warming in the equatorial central Pacific, whereas El Niño Modoki II displays an asymmetric distribution with the warm SST anomalies extending from the northeastern Pacific to equatorial central Pacific.

The composited SST anomalies of Fig. 4 in Wang and Wang (2013) show that there are cold SST anomalies in the southeastern tropical Indian Ocean for canonical El Niño and El Niño Modoki I, but warm SST anomalies for El Niño Modoki II although the paper of Wang and Wang (2013) does not focus on the variations in the Indian Ocean. This suggests that canonical El Niño and El Niño Modoki I may tend to relate to a positive IOD, whereas El Niño Modoki II is associated with a negative IOD. The purpose of the present paper is to examine and compare the relationships of the various groups of El Niño events with the IOD, and to investigate why some of El Niño Modoki events can induce a positive IOD, but some cannot. The paper is organized as follows. Section 2 introduces the data sets used in the study. Section 3 reveals the relationships of the IOD with the various groups of El Niño events, followed by the illustration of air-sea coupled processes associated with the IOD during various El Niño events in Section 4. Section 5 examines El Niño-related atmospheric circulations in the tropical Indo-Pacific, and explains the physical mechanism of why the various groups of El Niño events can result in different response of the IOD. Finally, Section 6 provides a summary and discussion.

2. Data sets

Observational data are relatively reliable after the second half of the 20th century, so this paper uses data after 1950. Several observational and reanalysis data sets are used in this study. The monthly atmospheric data sets include the newly developed NOAA Earth System Research Laboratory (ESRL) 20th Century Reanalysis (20CR) with a resolution of 2.0°×2.0° (Compo et al. 2011) during 1950-2010, and the Climate Prediction Center Merged Analysis of Precipitation (CMAP) (Xie and Arkin 1997) with a resolution of 2.5°×2.5° during 1979-2009. To confirm the results from the 20CR reanalysis data set, we also analyze the NCEP/NCAR reanalysis data set. During 1950-2008, the two reanalysis data sets show similar results. We present the results from the 20CR reanalysis in this paper. The oceanic data sets used in this study are the monthly SST from the Hadley Centre Sea Ice and SST data set (HadISST) on a 1°×1° resolution (Rayner et al. 2003) during 1950-2010, and subsurface temperature data from the Simple Ocean Data Assimilation (SODA version 2.1.6) (Carton and Giese, 2008) during 1958-2008. Since the SODA data end in 2008, the time period of all data sets analyzed in this study is from 1950 and 2008, except for CMAP which is from 1979-2008. Monthly mean data are smoothed with a 3-month running average to suppress subseasonal variability.

According to the definition of Saji et al. (1999), the IOD index is constructed by the SST anomaly gradient between the western equatorial Indian Ocean (50°E-70°E, 10°S-10°N) and the south eastern equatorial Indian Ocean (90°E-110°E, 10°S-0°N). The NINO3 index is the mean SST anomalies in the equatorial eastern-central Pacific (150°W-90°W, 5°S-5°N). The El Niño Modoki Index (EMI) is defined by Ashok et al. (2007) as:

$$\mathrm{EMI} = [\mathrm{SSTA}]_C - 0.5\times[\mathrm{SSTA}]_E - 0.5\times[\mathrm{SSTA}]_W,$$

where the brackets with a subscript represent the area-averaged SST anomalies over the central Pacific region C (165°E-140°W, 10°S-10°N), the eastern Pacific region E (110°W-70°W, 15°S-5°N) and the western Pacific region W (125°E-145°E, 10°S-20°N), respectively.

3. Relationships of the IOD with various groups of El Niño

The lead-lag correlations of the IOD index with the NINO3 and EMI indices are shown in Fig. 1. In this plot, the IOD peak season of boreal autumn (Sept-Oct-Nov, SON) is represented by the zero lag or month 0. The IOD index shows significant correlations with NINO3 when the NINO3 index leads up to six months, indicating the ENSO impact on the IOD (Behera and Yamagata 2003; Annamalai et al. 2003; Scott et al. 2009). The IOD index has a peak correlation with the EMI when the latter leads by 1-2 months, suggesting that El Niño Modoki during late summer and early autumn links with the IOD in the following autumn. On the other hand, Fig. 1 also suggests the distinct impacts of the IOD on canonical El Niño and El Niño Modoki. The IOD index is significantly correlated with NINO3 when the IOD index leads the NINO3 index up to five months, supporting the observed results that the IOD can influence greatly the changes of canonical El Niño in the growth and decay phases (Annamalai et al. 2005; Kug and Kang 2006). In contrast, there is rather weak and insignificant relationship between the autumn IOD and the lagged EMI, indicating that the IOD may not remotely influence El Niño Modoki events. In this study, we focus on different impacts of the various groups of El Niño events on the IOD, and influences of the IOD on canonical El Niño and El Niño Modoki will be examined in future studies.

Based on the opposite influence on rainfall in southern China and typhoon landfall activity, Wang and Wang (2013) classify and name El Niño Modoki I and II. By this

classification, El Niño Modoki I and II show different origins and patterns of SST anomalies. The warm SST anomalies originate in the equatorial central Pacific and subtropical northeastern Pacific for El Niño Modoki I and II, respectively. El Niño Modoki I shows a symmetric SST anomaly distribution about the equator with the maximum warming in the equatorial central Pacific, whereas El Niño Modoki II displays an asymmetric distribution with the warm SST anomalies extending from the northeastern subtropical Pacific to equatorial central Pacific. In this paper, we plot the SST anomaly distributions for all El Niño Modoki events during 1950-2008. We then inspect every event and identify El Niño Modoki I and II according to the characteristics of SST anomalies described by Wang and Wang (2013). Since ENSO is phase-locked to the seasonal cycle, only the years in which the warm SST anomalies exceed 0.5°C during July to November (JASON) and persist during December to February (DJF) are considered to be El Niño Modoki. If the warm SST anomalies during JASON locate in the tropical Pacific west to 140°W and are symmetric to the equator, it is recorded as El Niño Modoki I. If the maximum of warm SST anomalies during JASON locates in the northeastern subtropical Pacific and warm SST anomalies tilt from the northeastern subtropical Pacific to the central equatorial Pacific, it is labeled as El Niño Modoki II. By doing so, El Niño Modoki I and II during 1950-2008 are identified and are listed in Table 1. The years of El Niño Modoki I and II in Table 1 are the same as those of Wang and Wang (2013) except 1991 and 1958. Here, 1991 is considered as El Niño Modoki I because the center of warm SST anomalies is located in the central tropical Pacific (west to 150°W). 1958 is added for El Niño Modoki II in this paper because the maximum of warm SST anomalies locates in the northeastern subtropical Pacific during JASON in 1958. Although the SST anomalies exceed 0.5°C in the central tropical Pacific

in 1958, the warm area is small. Therefore, this 1958 event is hardly captured by several El Niño Modoki indices (e.g., Ashok et al. 2007; Kao and Yu 2009; Ren and Jin 2011).

Table 1 shows El Niño events and the intensity of the associated IOD during its peak phase of boreal autumn. Here, canonical El Niño is defined by the NINO3 SST anomalies such that the 5-month running mean NINO3 SST anomalies are +0.5ºC or higher for six consecutive months or longer (Wang and Wang 2013). From Table 1, most of canonical El Niño events are accompanied by the positive IOD except for 1957. Similar to canonical El Niño events, all El Niño Modoki I events are associated with the positive IOD. In contrast, most of El Niño Modoki II events except for 2004 are in association with the negative IOD. Because El Niño Modoki events can be associated with either a positive or negative IOD event, the correlation between the EMI and the IOD indices is not high as shown in Fig. 1.

Based on the El Niño years in Table 1, we compute the composited SST anomaly evolutions in the tropical Indo-Pacific from the onset phase to the mature phase for three groups of El Niño events (Fig. 2). As shown in Wang and Wang (2013), the warm SST anomalies of canonical El Niño firstly appear in the eastern tropical Pacific along the South American coast during spring, and then propagate westward (the left column of Fig. 2). Because of strong air-sea coupled processes in the tropical Pacific, the warm SST anomalies are gradually enhanced and reach the maximum in the following summer to winter. The cold SST anomalies are developed simultaneously in the western tropical Pacific. In the Indian Ocean, the positive IOD pattern firstly occurs in summer, peaks in autumn, and disappears in winter. In contrast, the composites of warm SST anomalies of El Niño Modoki events do not originate from the South American coast. For El Niño Modoki I (the middle column of Fig. 2), the warm SST anomalies occur in the central Pacific along the equator in summer in consistent with the results of Yu and

Kim (2010), accompanying with the positive IOD pattern. The warm SST anomalies are gradually intensified and reach the peak in the central tropical Pacific during autumn and winter, while the positive IOD maintains in autumn, and disappears in winter. For El Niño Modoki II (the right column of Fig. 2), the warm SST anomalies are firstly seen in the northeastern subtropical Pacific in spring, further develop extending to the equatorial central Pacific in summer and autumn, and reach maximum in winter. Different from the co-occurring positive IOD in canonical El Niño and El Niño Modoki I, there is a clearly negative IOD pattern firstly seen during summer in El Niño Modoki II, which persists in autumn and disappears in winter. Therefore, the distinguished feature in the Indian Ocean is that a negative IOD co-occurs with El Niño Modoki II during El Niño developing year, whereas a positive IOD is associated with canonical El Niño and El Niño Modoki I. In the next section, we will investigate the ocean-atmosphere coupled processes associated with the IOD during various El Niño events.

4. Ocean-atmosphere coupling of the IOD associated with various El Niño events

The Bjerknes feedback is critical for the growth and development of the IOD, especially in the eastern Indian Ocean off Java-Sumatra (e.g., Saji et al. 1999; Webster et al. 1999; Schott et al. 2009; Liu et al. 2011). In order to explore ocean-atmosphere coupled processes in the Indian Ocean associated with various El Niño events, we analyze the atmosphere-thermocline processes in the eastern tropical Indian Ocean involving precipitation, surface wind, sea level pressure (SLP) and thermocline depth during El Niño developing year. The 20°C isothermal depth is used as a proxy for thermocline depth as in previous studies (e.g., Xie et al. 2002).

For canonical El Niño, the significantly negative precipitation anomalies are seen in the eastern Indian Ocean in spring, and a strong east-west contrast of precipitation anomalies is

shown during October and November (Fig. 3a). Forced by the heating sink associated with the negative precipitation anomalies in the eastern tropical Indian Ocean, an anticyclone develops as a Rossby-wave response in the southeastern Indian Ocean (Gill 1980), which induces upwelling-favorable easterly anomalies off Java-Sumatra since July (Fig. 4a). The anomalous easterlies can result in the significantly shallow thermocline off Java-Sumatra (Fig. 5a). The shallow thermocline leads to enhancement of cool SST anomalies via upwelling of anomalous cold subsurface water in the eastern Indian Ocean, which further suppresses the convection precipitation (Fig. 3a) and amplifies the easterly anomalies in late summer and autumn (Fig. 4a). Through this positive dynamical feedback, the positive IOD develops and maintains (the left column of Fig. 2). This atmosphere-thermocline coupled feedback in the eastern Indian Ocean is also operated for El Niño Modoki I although there are few differences. Compared with the conditions of canonical El Niño, the amplitudes of precipitation and thermocline depth anomalies are weak for El Niño Modoki I, which may be attributed to the weaker warm SST anomalies in the tropical Pacific (Fig. 2).

In contrast, the positive precipitation anomalies appear in the eastern Indian Ocean since April and are the strongest during August and September for El Niño Modoki II (Fig. 3c). These convective diabatic heating forms the cyclone anomalies at the sea surface in terms of Gill-Matsuno dynamics (Gill 1980) and the resultant westerly anomalies over the eastern Indian Ocean in summer and autumn (Fig. 4c). The westerly wind anomalies deepen the thermocline (Fig. 5c) and are favorable for warm SST anomalies (the right column of Fig. 2) off Java-Sumatra. The warm SST anomalies in turn enhance the convective activity and westerly wind anomalies. Consequently, a negative IOD is developed during El Niño Modoki II (the right column of Fig. 2).

5. Variations of the Walker circulation associated with various El Niño events

The anomalous SST patterns in the tropical Pacific can induce the variations of wind and rainfall anomalies in the Indo-Pacific in associated with the Walker circulation variation. It is known that an El Niño is able to initiate an IOD through a weakening of the Walker circulation (Annamalai et al. 2003; Gualdi et al. 2003; Vecchi and Soden 2007). Our analyses in last section show that the various groups of El Niño events induce the different IOD patterns in association with the ocean-atmosphere coupling. In this section, we examine the large-scale atmospheric circulation anomalies that link the various groups of El Niño events with the IOD. Because of the strong seasonality of the IOD and its relationship with El Niño (Fig. 1), we focus on the large-scale atmospheric circulation anomalies in the tropical Indo-Pacific during July to November (JASON).

The spatial distributions of the precipitation anomalies during JASON in the tropical Indo-Pacific for the three types of El Niño events are shown in Fig. 6. In general, there is a clear dipole pattern with the negative precipitation anomalies in the eastern Indian Ocean and the western tropical Pacific, and the positive precipitation anomalies in the central and eastern tropical Pacific for canonical El Niño and El Niño Modoki I. The amplitude of precipitation anomalies for canonical El Niño is larger than that for El Niño Modoki I. However, the spatial pattern of the precipitation anomalies for El Niño Modoki II is clearly distinct, which show the positive precipitation anomalies in the west coast of Java-Sumatra and the western tropical Pacific, and the negative precipitation anomalies in the tropical maritime continent (Fig. 6c).

Due to the different patterns of the precipitation anomalies, it is expected that the large-scale atmospheric circulation over the tropical Indo-Pacific is different for the various groups of

El Niño events. At the low-level, all of three groups of El Niño events are generally characterized by the SLP anomalies of a see-saw pattern between the Western and Eastern Hemispheres although the amplitudes of the SLP anomalies are different (Fig. 7). For El Niño Modoki II (Fig. 7c), the negative SLP anomaly center shifts northward to the subtropical North Pacific in association with the underlying anomalous SST warming (Fig. 2). Fig. 7 also features that the westerly wind anomalies appear in the tropical Pacific for all groups of El Niño. Compared with canonical El Niño, the westerly wind anomalies in the tropical Pacific are weaker, and shift westward for El Niño Modoki I and II (Fig. 7). Although all groups of El Niño events show the positive SLP anomalies in the Indian Ocean, the distinguished differences are still featured by the east-west gradient of SLP anomalies and wind anomalies. The anomalous SLP anomalies for canonical El Niño and El Niño Modoki I in the tropical Indian Ocean are characterized by the anomaly higher in the eastern Indian Ocean and lower in the western Indian Ocean (Figs. 7a and 7b). The positive SLP anomaly centers in the southeast tropical Indian Ocean locate roughly 20° to the southwest of center of the heating sink shown in Fig. 6, confirming the Rossby-wave response (Gill 1980). The anomalous anticyclone therefore enhances the surface easterly wind anomalies off Java-Sumatra in favorable of triggering and developing the positive IOD (Yu et al. 2005). For El Niño Modoki II (Fig. 7c), the SLP anomaly in the western Indian Ocean is higher than that in the eastern Indian Ocean, indicating the east-west SLP gradient in the tropical Indian Ocean is opposite to these for canonical El Niño and El Niño Modoki I. This SLP anomaly pattern in the Indian Ocean is favorable for the westerly wind anomalies in the eastern tropical Indian Ocean. The enhancement of the anomalous westerly wind off Java-Sumatra piles up warm surface water in the eastern Indian Ocean and thus tends to form a negative IOD event.

At the high-level, the composite velocity potential and divergent wind anomalies for three groups of El Niño are displayed in Fig. 8. Centers of the positive (negative) velocity potential are associated with the anomalous convergent inflow (divergent outflow) winds. Upper troposphere velocity potential anomalies for canonical El Niño and El Niño Modoki I show the convergence in the eastern tropical Indian Ocean and divergence in the tropical Pacific. It is noted that the location of the divergence center for El Niño Modoki I shifts westward in comparison with that for canonical El Niño. However, for El Niño Modoki II, the equatorial western Indian Ocean shows an anomalous convergence, whereas the equatorial eastern Indian Ocean displays an anomalous divergence (Fig. 8c).

These results suggest that the three groups of El Niño events are associated with different atmospheric circulation patterns. It has been previously suggested that the eastern tropical Pacific warming forces the IOD via the Walker circulation variation (e.g., Baquero-Bernal et al. 2002; Annamalai et al. 2003; Fischer et al. 2005; Vecchi and Soden 2007). Here we analyze and compare the Walker circulations for the three groups of El Niño events. To clearly illustrate the changes of the Walker circulation, we firstly show climatology of the Walker circulation over the Indo-Pacific during July to November (Fig. 9). Climatologically, the ascent motion branches of the Walker circulation locate across the eastern tropical Indian Ocean and the western tropical Pacific (60°-180°E), and the descent motion branches are over the western tropical Indian Ocean and the eastern tropical Pacific (Fig. 9).

The anomalous atmospheric circulations for the three groups of El Niño events are composited in Fig. 10. For canonical El Niño, atmospheric circulation pattern manifests a weakening of the Walker circulation. In Fig. 10a, air anomalously rises in the eastern tropical Pacific (east of 180°E) because of underlying SST warming, flows westward aloft, sinks in the

western tropical Pacific and the eastern Indian Ocean. This circulation cell produces the easterly wind anomalies in the eastern tropical Indian Ocean and the westerly anomalies in the western/central tropical Pacific at the lower troposphere. The descent branches of the anomalous Walker circulation decrease precipitation and enhance the surface easterly wind anomalies in the eastern tropical Indian Ocean, which support the onset and development of a positive IOD. The anomalous Walker circulations induced by El Niño Modoki I (Fig. 10b) are similar to these by canonical El Niño but the intensities are weaker, and thus a positive IOD is also expected to be forced.

However, the zonal circulation anomalies associated with the El Niño Modoki II over the tropics (Fig.10c) are distinct from these of canonical El Niño and El Niño Modoki I, especially in the tropical Indian Ocean. Over the tropical Pacific, the center of ascent motion branch shifts westward during the El Niño Modoki II than these during canonical El Niño and El Niño Modoki I. The most remarkable difference is that the ascent motion branch appears over the tropical eastern Indian Ocean (center around 90°E) and the descent motion in the western tropical Indian Ocean (center around 60°E) during El Niño Modoki II. The ascent and descent motion is consistent with the upper troposphere divergence and convergence in the Indian Ocean (Fig. 8c). From Fig. 7c, the higher SLP anomalies associated with El Niño Modoki II shift further westward in the Pacific and are centered around 20°N, which produce the northeasterly wind anomalies across the South China Sea and reach the eastern tropical Indian Ocean. These northeasterly wind anomalies meet the westerly wind anomalies over the eastern Indian Ocean, resulting in the lower convergence and the positive rainfall anomalies (Fig. 6c) over there and inducing the anomalous ascent motion branch of the Walker circulation over the eastern tropical Indian Ocean (Fig. 10c). The anomalous Walker circulation in the Indian Ocean associated with

El Niño Modoki II produces the lower-level westerly wind anomalies in the eastern tropical Indian Ocean which are favorable to generate a negative IOD event in terms of the Bjerknes feedback.

6. Summary and discussion

Many studies have separated El Niño into canonical El Niño and El Niño Modoki because their locations of maximum SST anomalies are different. The NINO3 index and El Niño Modoki index (EMI) have significant correlations with the IOD when the IOD lags, consistent with that the IOD is developed following an El Niño (Nagura and Konda 2007). As shown in this paper, some El Niño Modoki events lead to a positive IOD, while others result in a negative IOD. Because of this relationship, the correlation between the EMI and IOD indices is not high although it is statistically significant when El Niño Modoki leads. The IOD index is also significantly correlated with the NINO3 index when the IOD leads by up to five months, consistent with previous model results that the Indian Ocean variability can induce changes in NINO3 SST variability both in amplitude and period (Yu et al. 2002; Wu and Kirtman 2004). However, the correlation between the IOD and the lagged EMI is not significant, suggesting that the occurrence and maintenance of El Niño Modoki is weakly forced by the Indian Ocean variability.

El Niño Modoki events are further separated into El Niño Modoki I and II because they show different impacts on rainfall in southern China and the typhoon tracks in the western North Pacific (Wang and Wang 2013). El Niño Modoki I and II also show different origins and patterns of SST anomalies. Similar to canonical El Niño, El Niño Modoki I is associated with an anomalous anticyclone in the Philippine Sea which induces southwesterly wind anomalies along

the south coast of China and carries the moisture for increasing rainfall in southern China. For El Niño Modoki II, an anomalous cyclone resides east of the Philippines, associated with northerly wind anomalies and a decrease in rainfall in southern China. Canonical El Niño and El Niño Modoki I are associated with a westward extension of the western North Pacific subtropical high, whereas El Niño Modoki II shifts the western North Pacific subtropical high eastward. Differing from canonical El Niño and El Niño Modoki I, El Niño Modoki II corresponds to northwesterly anomalies of the typhoon steering flow which are unfavorable for typhoons to make landfall in China.

Following Wang and Wang's (2013) classification, the present paper investigates the influences of the various groups of El Niño events on the IOD. By inspecting the SST anomalies of all El Niño events during 1950-2008, we identify canonical El Niño, El Niño Modoki I and and II based on the SST anomaly patterns in the tropical Pacific as described in Wang and Wang (2013). For canonical El Niño, the warm SST anomalies originate along the coast of South America in the boreal spring, and then propagate toward the central tropical Pacific with the maximum warming SST anomalies in the eastern tropical Pacific. A positive IOD during summer and autumn tends to co-occur with a canonical El Niño event. The warm SST anomalies for El Niño Modoki I abruptly appear in the central tropical Pacific symmetric to the equator in summer, intensify and reach the peak in the equatorial central Pacific. Similar to canonical El Niño, a positive IOD is also seen in the Indian Ocean during summer and autumn, and disappears in winter. However, for El Niño Modoki II, the warm SST anomalies originate in the northeastern subtropical Pacific in spring, and further develop reaching the equatorial central Pacific in summer and autumn. The warm SST anomaly pattern in the tropical Pacific is characterized to be asymmetric to the equator with the maximum in the subtropical northeastern

Pacific during summer and autumn. Accompanied with the El Niño Modoki II, a negative IOD is seen in summer and autumn, which is opposite to the conditions of canonical El Niño and El Niño Modoki I. In summary, canonical El Niño and El Niño Modoki I are related to a positive IOD, whereas El Niño Modoki II is associated with a negative IOD.

The present paper uses various observational data sets with different data periods, and we thus have to focus on the analyses starting from the middle 20th century. As shown in Table 1, the numbers of El Niño Modoki I and II are not too many. To increase their numbers, we extend the SST data to a longer period during 1910-2008. There are four more canonical El Niño events (1911/1912, 1918/1919, 1925/1926, and 1930/1931), which are associated with the IOD intensities of -0.5, 1.2, 1.4, and -0.2, respectively. For El Niño Modoki I, three more events are found (1914/1915, 1940/1941, and 1941/1942), which correspond to the IOD intensities of 0.2, -0.2, and 0.6, respectively. No more El Niño Modoki II is found for the longer period. Figure 11 shows the composite SST anomaly evolutions in the tropical Indo-Pacific for three groups of El Niño events during 1910-2008. The patterns of the composite SST anomalies during canonical El Niño and El Niño Modoki I are similar to these in Fig. 2, suggesting that most canonical El Niño and El Niño Modoki I are associated with the positive IOD and the results are robust independent on the length of data sets.

We further examine the ocean-atmosphere feedback process in the Indian Ocean by analyzing the co-variations of SST, surface wind, precipitation, and thermocline depth. For canonical El Niño and El Niño Modoki I, the precipitation anomalies over the eastern Indian Ocean are less than normal since summer. Therefore, the anomalous surface easterly wind occurs in the southeastern tropical Indian Ocean, which shallows the thermocline off Java-Sumatra. The shallowed thermocline enhances the SST cooling via upwelling of anomalous cold

subsurface water, which in turn suppresses the convection precipitation and amplifies the surface easterly wind anomalies. Canonical El Niño and El Niño Modoki I, assisted with the ocean-atmosphere coupling, thus lead to a positive IOD. In contrast, for El Niño Modoki II, the positive precipitation and surface westerly wind anomalies are located in the southeastern Indian Ocean, resulting from the different influence from the Pacific by the Walker circulation. Oceanic and atmospheric conditions for El Niño Modoki II are opposite to those of canonical El Niño and El Niño Modoki I. As a result, a negative IOD appears in the Indian Ocean on the frame of the Bejerknes feedback during El Niño Modoki II.

The positive and negative IOD during the various groups of El Niño events are induced by the different changes of the Walker circulation. Similar to previous studies that canonical El Niño influences the IOD onset through a weakened Walker circulation (Annamalari et al. 2003; Vecchi and Soden 2007), El Niño Modoki I also induces a weakening of the Walker circulation. The weakened Walker circulation results in less precipitation across the eastern tropical Indian Ocean and maritime continent and more in the eastern tropical Pacific. The descent branches of the anomalous Walker circulation and heating sink-induced response in the eastern tropical Indian Ocean lead to the surface easterly wind anomalies. Through coupled atmosphere-thermocline feedback, the SST anomalies are cooler and cooler in the eastern tropical Indian Ocean, and thus a positive IOD occurs. However, El Niño Modoki II-induced Walker circulation is different from these during canonical El Niño and El Niño Modoki I. The ascent motion around 90°E enhances convective activity and brings more precipitation in the west coast of Sumatra. Based on the Gill theory (1980), these heating anomalies induce a pair of cyclone along the equator, which produces the surface westerly wind anomalies. Under the Bjerknes feedback, SST anomalies are warm and thermocline is deepened off Java-Sumatra, which in turn

1 further enhances westerly wind anomalies. Consequently, a negative IOD pattern appears and
2 develops during El Niño Modoki II.
3 In the recent past three decades, the ENSO variability is changed (Cobb et al. 2003;
4 Wang et al. 2009), and the intensity and frequency of El Niño Modoki are increasing (Lee and
5 McPhaden 2010). The model results suggest that under a global warming scenario, El Niño
6 Modoki occurs more frequent than canonical El Niño (Yeh et al. 2009). Our present study
7 suggests that El Niño Modoki I and II have different impacts on Indian Ocean climate via the
8 distinct changes in the Walker circulation. Long-term changes in the Walker circulation have
9 recently been the subject of intense debate. Many studies showed the weakened Walker
10 circulation over the twentieth century (e.g., Vecchi et al. 2006; Power and Kociuba 2011;
11 Tokinaga et al. 2012). Some studies suggested that the tropical Pacific trade winds may have
12 strengthened over the past two decades (e.g., Merrifield 2011; Li and Ren 2012), and that the
13 Walker Cell has been enhanced in the past two decades (Luo et al. 2012). Therefore, the
14 influences of the relative changes of El Niño Modoki I and II on the long-term changes in the
15 Walker circulations are needed to analyze in the future. An examination of the relative changes
16 of El Niño Modoki I and II is also needed for improving the understanding and prediction of
17 Indian Ocean climate variability under future global warming.
18
19 *Acknowledgments*. We thank two anonymous reviewers for their comments and suggestions on
20 the manuscript. This work was supported by the National Oceanic and Atmospheric
21 Administration (NOAA) Climate Program Office, the base funding of NOAA Atlantic
22 Oceanographic and Meteorological Laboratory (AOML), the National Basic Research Program
23 of China (2013CB430301), and the Chinese Academy of Sciences. The findings and

conclusions in this report are those of the author(s) and do not necessarily represent the views of the funding agency.

References

Annamalai H, Murtugudde R, Potemra J, Xie SP, Liu P, Wang B (2003) Coupled dynamics over the Indian Ocean: Spring initiation of the zonal mode. Deep Sea Res II 50: 2305-2330

Annamalai H, Xie SP, McCreary JP, Murtugudde R (2005) Impact of Indian Ocean sea surface temperature on developing El Nino. J Clim 18: 302-319

Ashok K, Guan Z, Yamagata T (2003) Influence of the Indian Ocean Dipole on the Australian winter rainfall. Geophys Res Lett 30: 1821, doi: 10.1029/2003GL017926

Ashok K, Guan Z, Saji NH, Yamagata T (2004) Individual and combined influences of ENSO and Indian Ocean dipole on the Indian summer monsson. J Clim 17: 3134-3155

Ashok K, Behera SK, Rao SA, Weng H, Yamagata T (2007) El Niño Modoki and its possible teleconnection. J Geophys Res 112: C11007, doi: 10.1029/2006JC003798

Ashok K, Iizuka S, Rao SA, Saji NH, Lee WJ (2009) Processes and boreal summer impacts of the 2004 El Niño Modoki: An AGCM study. Geophys Res Lett 36: L04703, doi: 10.1029/2008GL036313

Baquero-Bernal A, Latif M, Legutke M (2002) On dipole like variability of sea surface temperature in the tropical Indian Ocean. J Clim 15: 1358-1368

Behera SK, Yamagata T (2003) Influence of the Indian Ocean dipole on the Southern Oscillation. J Meteorol Soc Jpn 81: 169-177

Behera SK, Luo JJ, Masson S, Rao SA, Sakumo H, Yamagata T (2006) A CGCM study on the interaction between IOD and ENSO. J Clim 19: 1608-1705

Cai W, Cowan T, Sullivan A (2009) Recent unprecedented skewness towards positive Indian Ocean Dipole occurrences and its impact on Australian rainfall. Geophys Res Lett 36: L11705, doi: 10.1029/2009GL037604

Carton JA, Giese BS (2008) A reanalysis of ocean climate using simple ocean data assimilation (SODA). Mon Weather Rev 136: 2999-3017

Cobb KM, Charles CD, Cheng H, Edwards RL (2003) El Niño/Southern Oscillation and tropical Pacific climate during the last millennium. Nature 424: 271-276

Compo GP, and Co-authors (2011) The Twentieth Century Reanalysis Project. Q J R Meteorol Soc 137: 1-28

Feng J, Chen W, Tam CY, Zhou W (2011) Different impacts of El Niño and El Niño Modoki on China rainfall in the decaying phases. Int J Climatol 31: 2091-2101

Fischer AP, Terray P, Guilyardi E, Gualdi S, Delecluse P (2005) Two independent triggers for the Indian Ocean Dipole zonal mode in a coupled GCM. J Clim 18: 3428-3449

Gill AE (1980) Some simple solutions for heat-induced tropical circulation. Q J R Meteorol Soc 106: 447-462

Gualdi S, Guilyardi E, Navarra A, Masina S, Delecluse P (2003) The interannual variability in the tropical Indian Ocean as simulated by a CGCM. Clim Dyn 20: 567-582

Hastenrath S (2002) Dipoles, temperature gradients, and tropical climate anomalies. Bull Amer Meteorol Soc 83: 735-740

Kao HY, Yu JY (2009) Contrasting eastern-Pacific and central-Pacific types of El Niño. J Clim 22: 615-632

Kim JS, Zhou W, Wang X, Jain S (2012) El Niño Modoki and the summer precipitation variability over South Korea: A diagnostic study. J Meteorol Soc Jpn 90: 673-684

Krishnamurthy V, Kirtman BP (2003) Variability of the Indian Ocean: Relation to monsoon and ENSO. Q J R Meteorol Soc 129: 1623-1646

Kug JS, Kang IS (2006) Interactive feedback between ENSO and the Indian Ocean. J Clim 19: 1784-1801

Kug JS, Jin FF, An SI (2009) Two types of El Niño events: Cold tongue El Niño and warm pool El Niño. J. Clim 22: 1499-1515

Larkin NK, Harrison DE (2005) Global seasonal temperature and precipitation anomalies during El Niño autumn and winter. Geophys Res Lett 32: L16705, doi: 10.1029/2005GL022860

Lau NC, Nath MJ (2004) Coupled GCM simulation of atmosphere ocean variability associated with the zonally asymmetric SST changes in the tropical Indian Ocean. J Clim 20: 4497-4525

Lee T, McPhaden MJ (2010) Increasing intensity of El Niño in the central-equatorial Pacific. Geophys Res Lett 37: L14603, doi: 10.1029/2010GL044007

Li CY, Zhou W, Jia XL, Wang X (2006) Decadal/Interdecadal variations of ocean temperature and its impacts on climate. Adv Atmos Sci 23: 964-981

Li G, Ren B (2012) Evidence for strengthening of the tropical Pacific Ocean surface wind speed during 1979-2001. Theor Appl Climatol 107:59–72.

Liu L, Yu W, Li T (2011) Dynamic and Thermodynamic Air-Sea Coupling Associated with the Indian Ocean Dipole Diagnosed from 23 WCRP CMIP3 Models. J Clim 24: 4941-4958, doi: 10.1175/2011JCLI4041.1

Luo JJ, Behera S, Masumoto Y, Sakuma H, Yamagata T (2008) Successful prediction of the consecutive IOD in 2006 and 2007. Geophys Res Lett 35: L14S02, doi: 10.1029/2007GL032793

Luo JJ, Zhang R, Behera S, Masumoto Y, Jin FF, Lukas R, Yamagata T (2010) Interaction between El Niño and extreme Indian Ocean dipole. J Clim 23: 726-742

Luo JJ, Sasaki W, Masumoto Y (2012) Indian Ocean warming modulates Pacific climate change. PNAS 109: 18701-18706

Merrifield MA (2011) A shift in western tropical Pacific sea-level trends during the 1990s. J Clim 24:4126–4138

Meyers G, McIntosh P, Pigot L, Pook M (2007) The years of El Niño, La Niña and interactions with the tropical Indian Ocean. J Clim 20: 2872-2880

Nagura M, Konda M (2007) The seasonal development of an SST anomaly in the Indian Ocean and its relationship to ENSO. J Clim 20: 38-52

Power SB, Kociuba G (2011) What caused the observed twentieth-centuryweakening of the Walker circulation? J Clim 24: 6501-6514

Rayner NA, and Co-authors (2003) Global analysis of sea surface temperature, sea ice and night marine air temperature since the late nineteenth century. J Geophys Res 108: 4407, doi:10.1029/2002JD002670

Ren HL, Jin FF (2011) Niño indices for two types of ENSO. Geophys Res Lett 38: L04704, doi: 10.1029/2010GL046031

Saji NH, Goswami BN, Vinayachandran PN, Yamagata T (1999) A dipole mode in the tropical Indian Ocean. Nature 401: 360-363

Saji NH, Yamagata T (2003) Possible impacts of Indian Ocean Dipole mode events on global climate. Clim Res 25: 151-169

Schott FA, Xie SP, McCreary J (2009) Indian Ocean circulation and climate variability. Rev Geophys 47: RG1002, doi: 10.1029/2007RG000245

Song Q, Vecchi GA, Rosati AJ (2007) Indian Ocean variability in the GFDL CM2 coupled climate model. J Clim 20: 2895-2916

Song Q, Vecchi GA, Rosati AJ (2008) Predictability of the Indian Ocean sea surface temperature anomalies in the GFDL coupled model. Geophys Res Lett 35: L02701, doi: 10.1029/2007GL031966

Tokinaga H, Xie SP., Deser C, Kosaka Y, Okumura YM (2012) Slowdown of the Walker circulation driven by tropical Indo-Pacific warming. Nature 491: 439-443

Ueda H, Matsumoto J (2001) A possible triggering process of east-west asymmetric anomalies over the Indian Ocean in relation to 1997/98 El Niño. J Meteorol Soc Jpn 7: 8803-8818

Vinayachandran PN, Saji NH, Yamagata T (1999) Response of the equatorial Indian Ocean to an anomalous wind event during 1994. Geophys Res Lett 26: 1613-1615

Vecchi GA, Soden BJ (2007) Global warming and the weakening of the tropical circulation. J Clim 20: 4316-4330

Vecchi GA, Soden BJ, Wittenberg AT, Held IM, Leetmaa A, Harrison MJ (2006) Weakening of tropical Pacific atmospheric circulation due to anthropogenic forcing. Nature 441: 73-76

Wang C, Wang X (2013) Classifying El Niño Modoki I and II by Different Impacts on Rainfall in Southern China and Typhoon Tracks. J Clim, in press, doi: 10.1175/JCLI-D-12-00107.1

Wang, C., Deser C, Yu J-Y, DiNezio P, Clement A (2013) El Niño-Southern Oscillation (ENSO): A review. In *Coral Reefs of the Eastern Pacific*, P. Glymn, D. Manzello, and I. Enochs, Eds., Springer Science Publisher, in press.

Wang X, Li C, Zhou W (2006) Interdecadal variation of the relationship between Indian rainfall and SSTA modes in the Indian Ocean. Int J Climatol 26: 595-606

Wang X, Wang D, Zhou W (2009) Decadal variability of twentieth century El Niño and La Niña occurrence from observations and IPCC AR4 coupled models. Geophys Res Lett 36: L11701, doi: 10.1029/2009GL037929

Webster PJ, Moore AM, Loschnigg JP, Leben RR (1999) Coupled ocean-atmosphere dynamics in the Indian Ocean during 1997-98. Nature 401: 356-360, doi: 10.1038/43848

Weng H, Ashok K, Behera SK, Rao SA, Yamagata T (2007) Impacts of recent El Niño Modoki on dry/wet conditions in the Pacific rim during boreal summer. Clim Dyn 29: 113-129

Wu R, Kirtman BP (2004) Understanding the impacts of the Indian Ocean on ENSO variability in a coupled GCM. J Clim 17: 4019-4031

Xiang B, Yu W, Li T, Wang B (2011) The critical role of the boreal summer mean state in the development of the IOD. Geophys Res Lett 38: L02710, doi: 10.1029/2010GL045851

Xie P, Arkin PA (1997) Global precipitation: A 17-year monthly analysis based on gauge observations, satellite estimates, and numerical model outputs. Bull Amer Meteorol Soc 78: 2539-2558

Xie SP, Annamalai H, Schott F, McCreary Jr JP (2002) Origin and predictability of South Indian Ocean climate variability. J Clim 15: 864-874

Yamagata T, Saji NH, Behera SK (2003) Comments on Indian Ocean dipole. Bull Amer Meteorol Soc 84: 1440-1442

Yeh SW, Kug JS, Dewitte B, Kwon MH, Kirtman BP, Jin FF (2009) El Niño in a changing climate. Nature 461: 511-515

Yu JY, Mechoso CR, McWilliams JC, Arakawa A (2002) Impacts of the Indian Ocean on the ENSO cycle. Geophys Res Lett 29: 1204, doi: 10.1029/2001GL014098

Yu JY, Kao HY (2007) Decadal changes of ENSO persistence barrier in SST and ocean heat content indices: 1958-2001. J Geophys Res 112: D13106, doi: 10.1029/2006JD007654

Yu JY, Kim ST (2010) Three evolution patterns of Central-Pacific El Niño. Geophys Res Lett 37: L08706, doi: 10.1029/2010GL042810

Yu W, Xiang B, Liu L, Liu N (2005) Understanding the origins of interannual thermocline variations in the tropical Indian Ocean. Geophys Res Lett 32: L24706, doi: 10.1029/2005GL024327

Yuan Y, Yang H, Zhou W, Li C (2008) Influences of the Indian Ocean dipole on the Asian summer monsoon in the following year. Int J Climatol 28: 1849-1859

Yuan Y, Yang S (2012) Impacts of Different Types of El Niño on the East Asian Climate: Focus on ENSO Cycles. J Clim 25: 7702-7722

Table and Figure Captions

Table 1. Various groups of El Niño events and corresponding SON-mean normalized IOD index values.

Figure 1. Lead-lag correlations of the IOD index with El Niño Modoki index (EMI) and NINO3 index during 1950-2008. The IOD index during Sept-Oct-Nov (SON) is represented by month 0 or zero lag. The dashed lines indicate 95% and 99% significant levels, respectively.

Figure 2. Evolution of composited SST anomalies for canonical El Niño (the left column), El Niño Modoki I (the middle column), and El Niño Modoki II (the right column). The first, second, third and fourth row represents the different El Niño phases of MAM (March[0] to May[0]), JJA (June[0] to August[0]), SON (September[0] to November[0]) and DJF (December[0] to February[+1]), respectively. The hatched represents the composite exceeding 90% significant level, which is calculated by Student's *t* test.

Figure 3. Composite precipitation (mm/day) anomalies averaged between 12°S-equator for different types of El Niño during their developing year. Shown are for (a) canonical El Niño, (b) El Niño Modoki I, and (c) El Niño Modoki II.

Figure 4. Composite 1000-hPa wind (vector, m/s), sea level pressure (shading, Pa) and zonal-mean (75°-100°E) surface zonal wind (lines, m/s) anomalies averaged between 12°S-equator for

different types of El Niño during their developing year. Shown are for (a) canonical El Niño, (b) El Niño Modoki I and (c) El Niño Modoki II.

Figure 5. Composites of the 20°C isothermal depth (m) anomalies averaged between 12°S-equator for different types of El Niño during their developing year. Shown are for (a) canonical El Niño, (b) El Niño Modoki I and (c) El Niño Modoki II. The hatched indicates the composite exceeding 90% significant level based on Student's *t* test.

Figure 6. Composites of JASON-mean precipitation (mm/day) anomalies for different types of El Niño. Shown are for (a) canonical El Niño, (b) El Niño Modoki I and (c) El Niño Modoki II.

Figure 7. Composites of JASON-mean 1000-hPa wind (vector, m/s) and SLP (shading, Pa) anomalies for different types of El Niño. Shown are for (a) canonical El Niño, (b) El Niño Modoki I and (c) El Niño Modoki II. Only the wind anomalies exceeding 0.4 m/s are plotted.

Figure 8. Composites of JASON-mean 200-hPa velocity potential (contour, 10^6 m^2 s^{-1}) and divergent wind (vector, m/s) anomalies for different types of El Niño. The zero contour line is thickened, and contour interval is 0.2 $\times 10^6$ m^2 s^{-1}. Shown are for (a) canonical El Niño, (b) El Niño Modoki I and (c) El Niño Modoki II.

Figure 9. The JASON-mean climatology of zonal-vertical circulation by averaging zonal component of divergent wind and vertical velocity (scaled by -100) between 10°S and 10°N. Shadings are pressure vertical velocity anomalies scaled by 100.

Figure 10. The streamline composites of JASON-mean zonal-vertical circulation anomalies by averaging zonal component of divergent wind and vertical velocity (scaled by -100) between 10°S and 10°N for different types of El Niño. Shown are for (a) canonical El Niño, (b) El Niño Modoki I and (c) El Niño Modoki II. The vectors indicate pressure vertical velocity exceeding 90% significant level based on Student's *t* test. Shadings are pressure vertical velocity anomalies scaled by 100.

Figure 11. Same as Fig. 2 except for using the longer-term data from 1910-2008. The composites are calculated from eleven canonical El Niño events (1911/12, 1918/1919, 1925/1926, 1930/1931, 1951/52, 1957/1958, 1965/66, 1972/73, 1976/77, 1982/83, and 1997/98), eight El Niño Modoki I events (1914/15, 1940/41, 1941/42, 1963/1964, 1987/88, 1990/91, 1991/1992, and 2002/03), and five El Niño Modoki II events (1958/1959, 1968/69, 1979/80, 1992/93, and 2004/05).

Table 1. Various groups of El Niño events and corresponding SON-mean normalized IOD index values.

Canonical El Niño	IOD	El Niño Modoki I	IOD	El Niño Modoki II	IOD
1951	0.6	1963	1.4	1958	-1.9
1957	-0.6	1987	1.2	1968	-0.85
1965	0.3	1990	0.1	1979	-0.1
1972	1.8	1991	0.7	1992	-1.0
1976	0.1	2002	1.3	2004	0.41
1982	1.8				
1997	3.2				

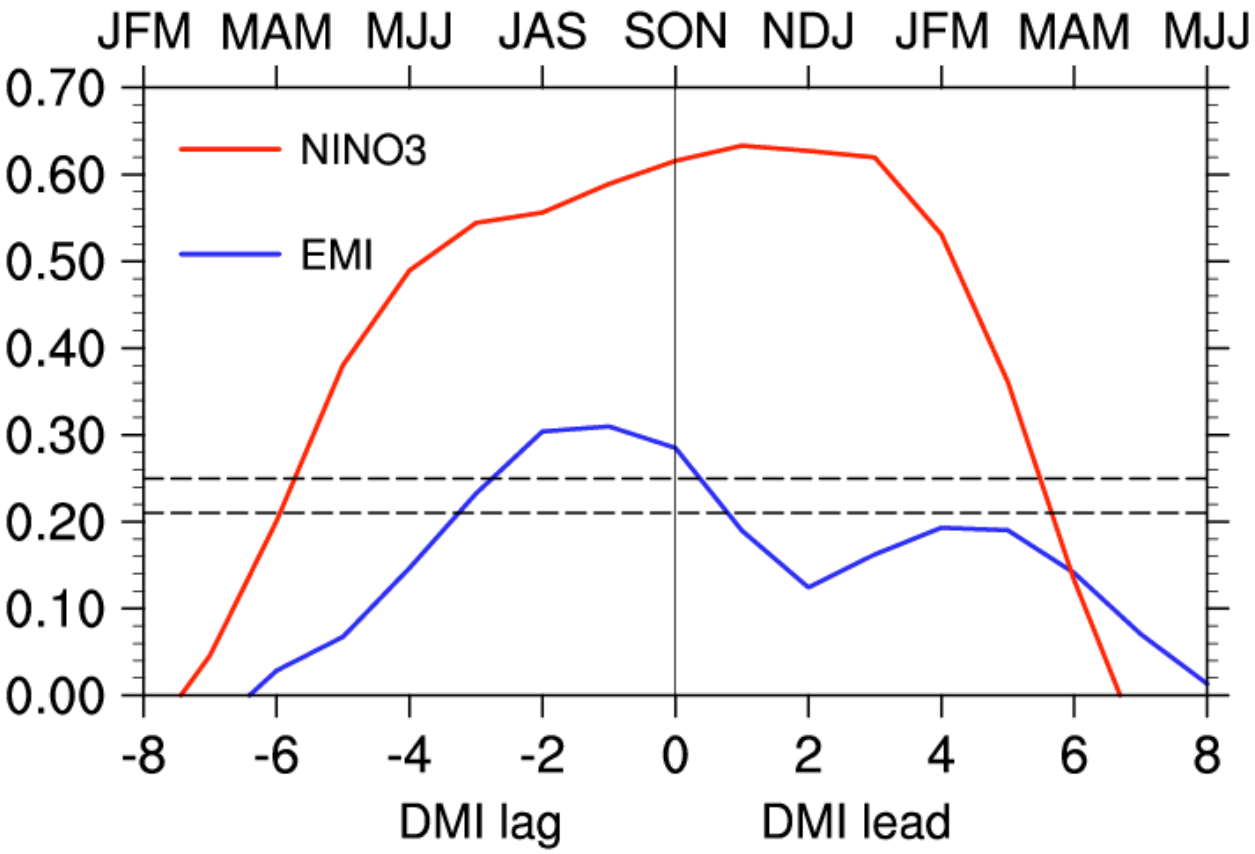

Figure 1. Lead-lag correlations of the IOD index with El Niño Modoki index (EMI) and NINO3 index during 1950-2008. The IOD index during Sept-Oct-Nov (SON) is represented by month 0 or zero lag. The dashed lines indicate 95% and 99% significant levels, respectively.

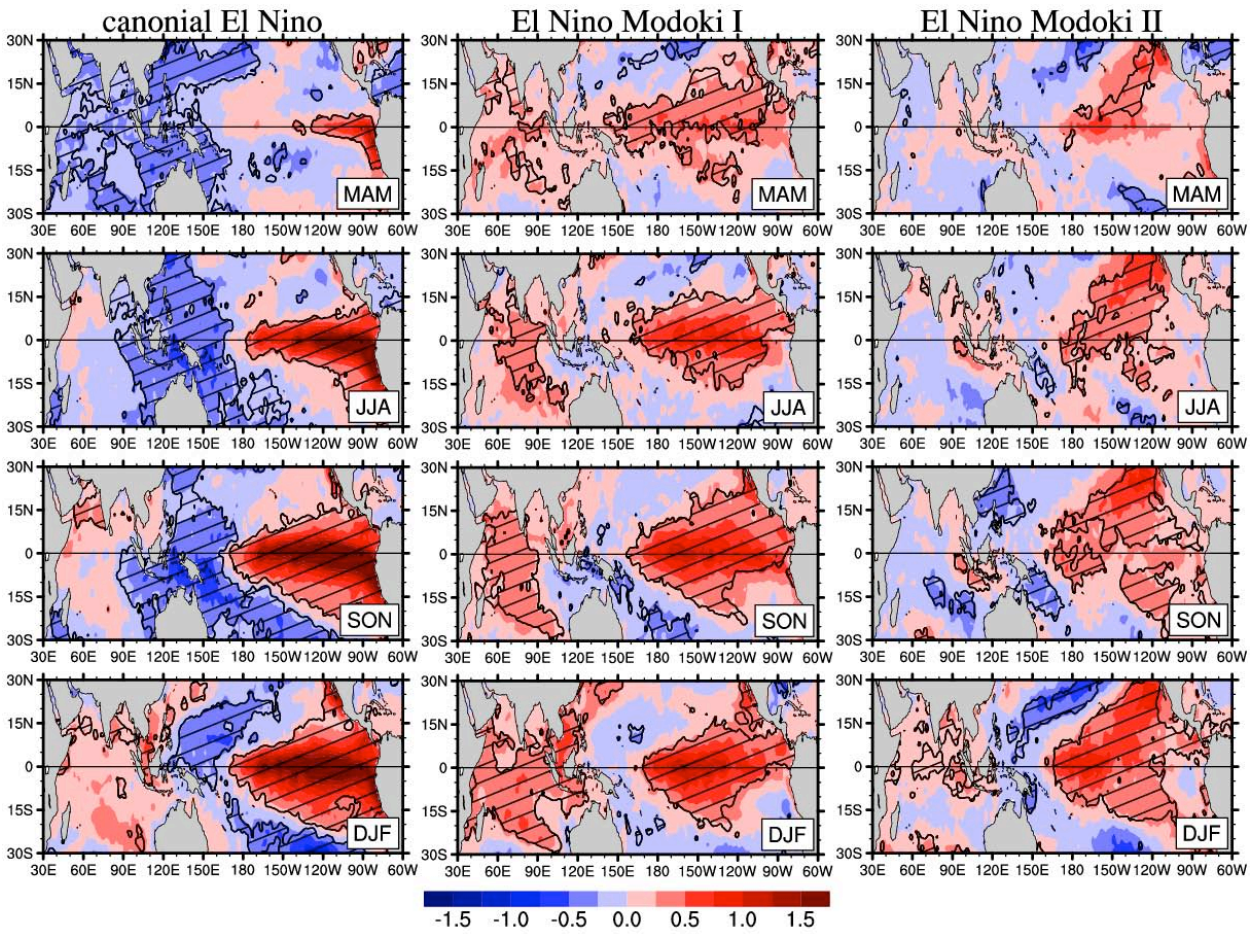

Figure 2. Evolution of composited SST anomalies for canonical El Niño (the left column), El Niño Modoki I (the middle column), and El Niño Modoki II (the right column). The first, second, third and fourth row represents the different El Niño phases of MAM (March[0] to May[0]), JJA (June[0] to August[0]), SON (September[0] to November[0]) and DJF (December[0] to February[+1]), respectively. The hatched represents the composite exceeding 90% significant level, which is calculated by Student's *t* test.

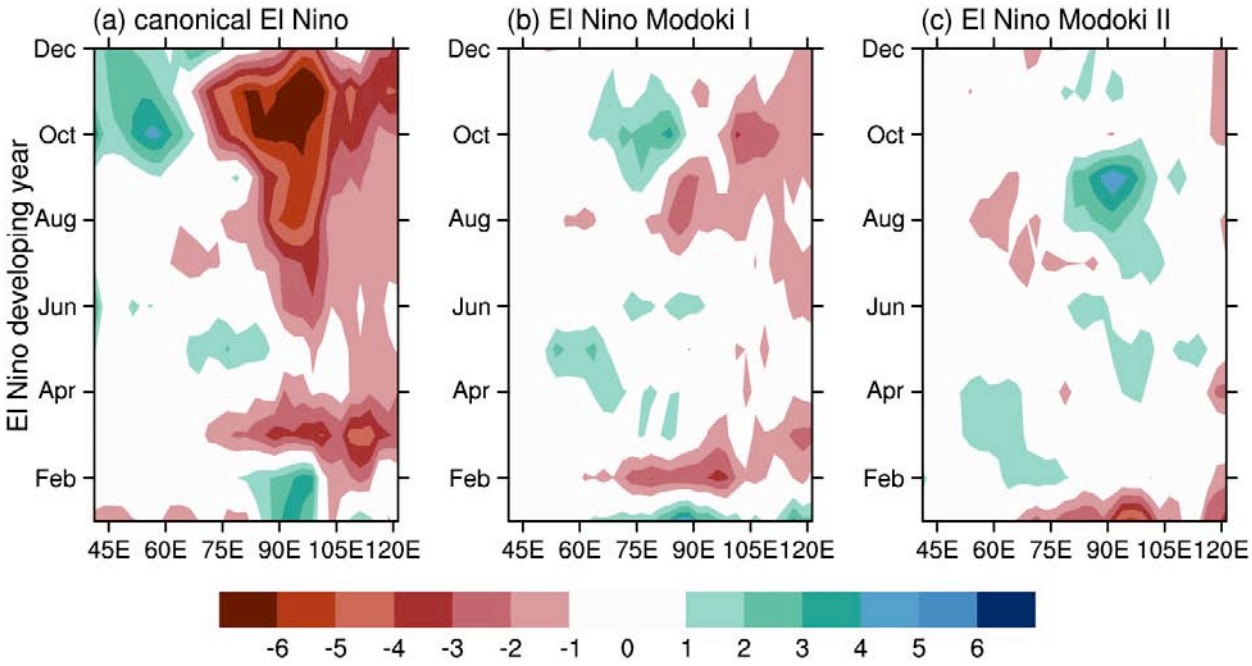

Figure 3. Composite precipitation (mm/day) anomalies averaged between 12°S-equator for different types of El Niño during their developing year. Shown are for (a) canonical El Niño, (b) El Niño Modoki I, and (c) El Niño Modoki II.

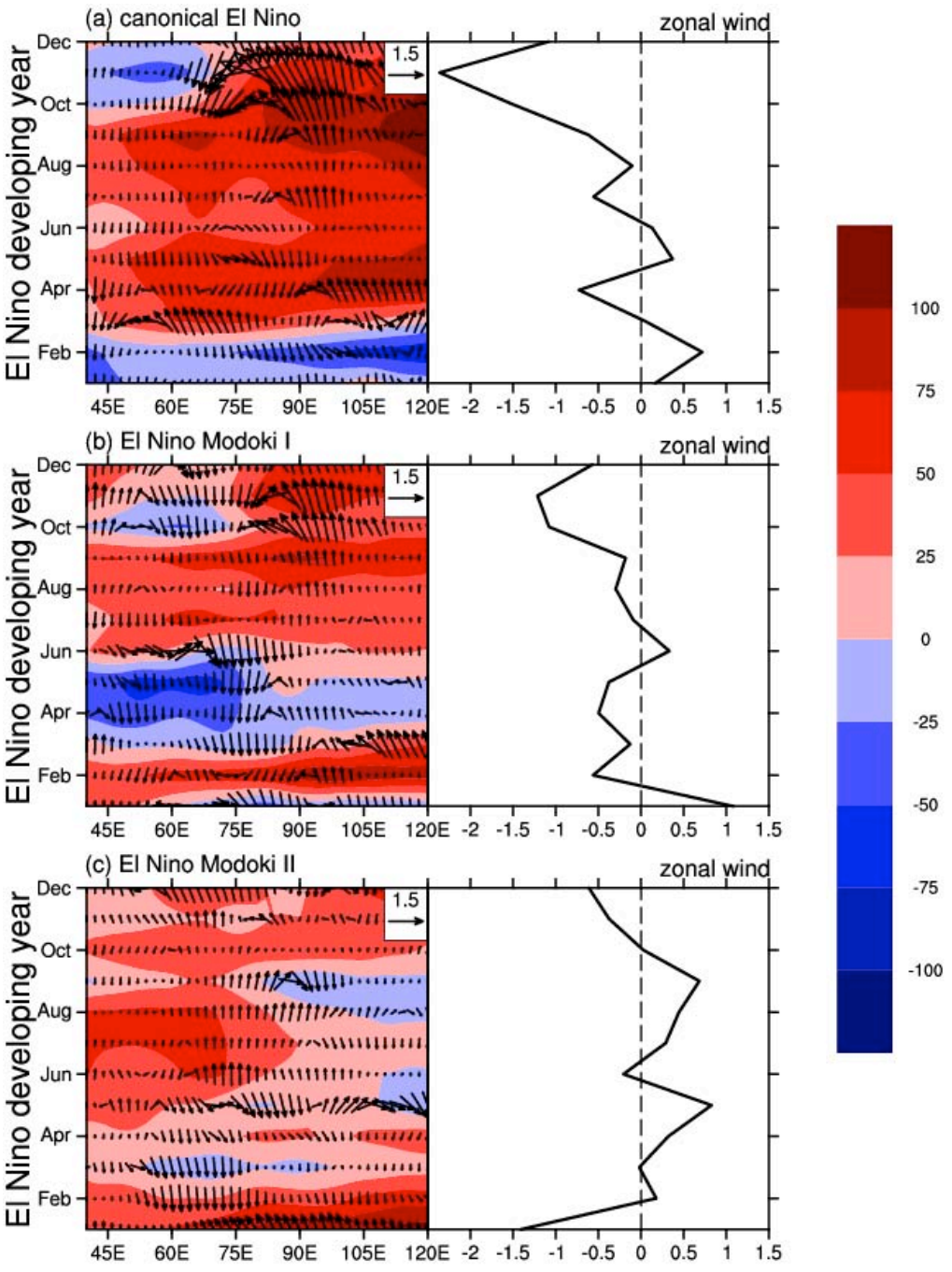

Figure 4. Composite 1000-hPa wind (vector, m/s), sea level pressure (shading, Pa) and zonal-mean (75°-100°E) surface zonal wind (lines, m/s) anomalies averaged between 12°S-equator for different types of El Niño during their developing year. Shown are for (a) canonical El Niño, (b) El Niño Modoki I and (c) El Niño Modoki II.

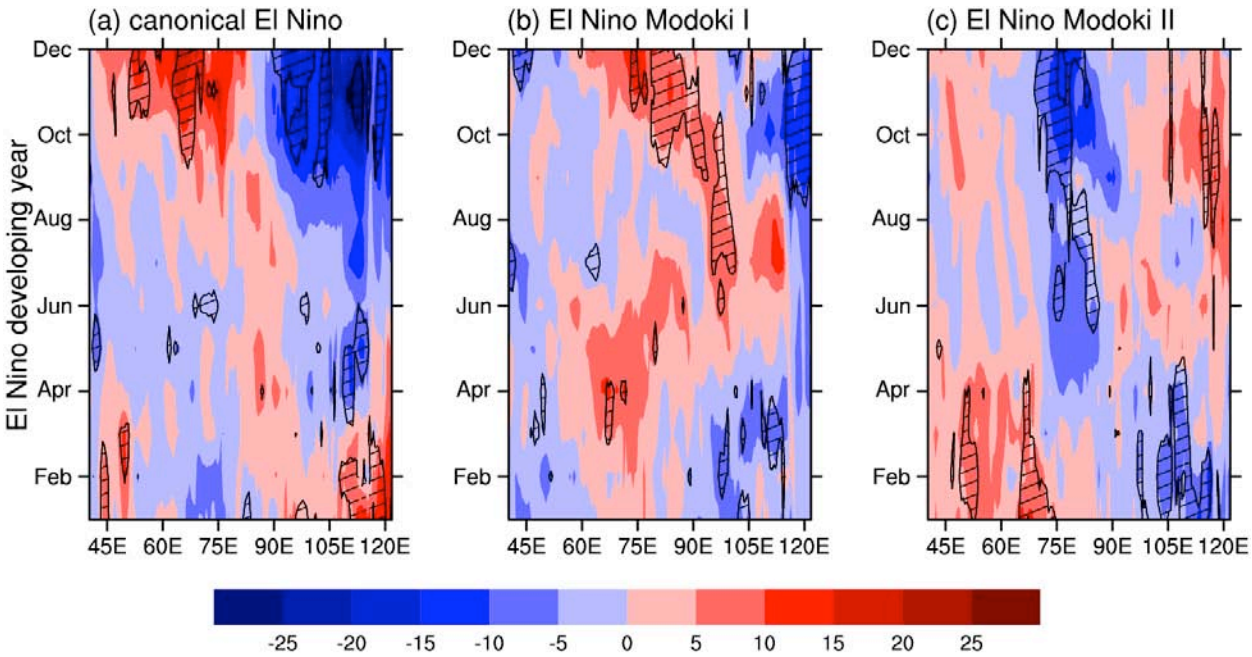

Figure 5. Composites of the 20°C isothermal depth (m) anomalies averaged between 12°S-equator for different types of El Niño during their developing year. Shown are for (a) canonical El Niño, (b) El Niño Modoki I and (c) El Niño Modoki II. The hatched indicates the composite exceeding 90% significant level based on Student's *t* test.

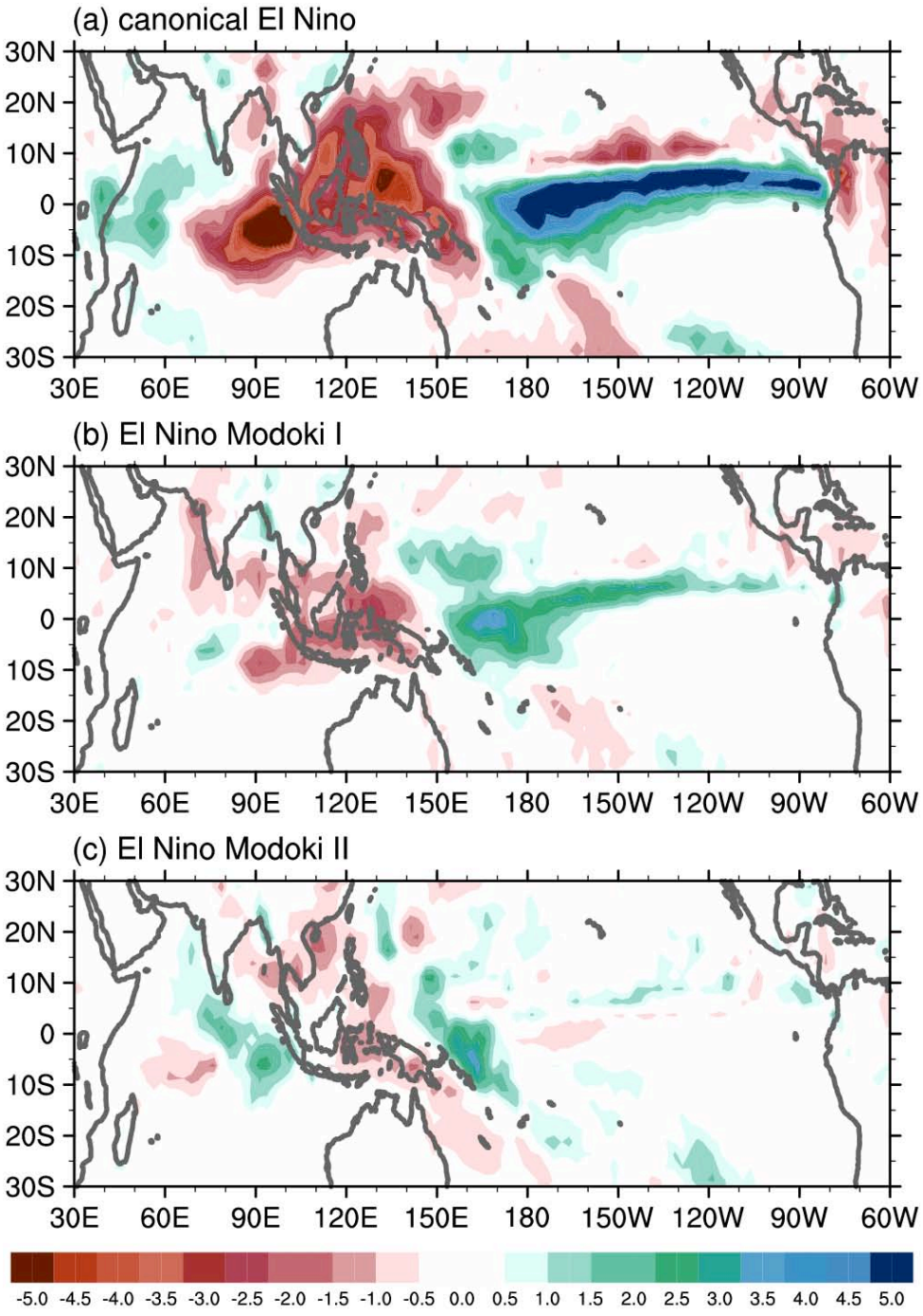

Figure 6. Composites of JASON-mean precipitation (mm/day) anomalies for different types of El Niño. Shown are for (a) canonical El Niño, (b) El Niño Modoki I and (c) El Niño Modoki II.

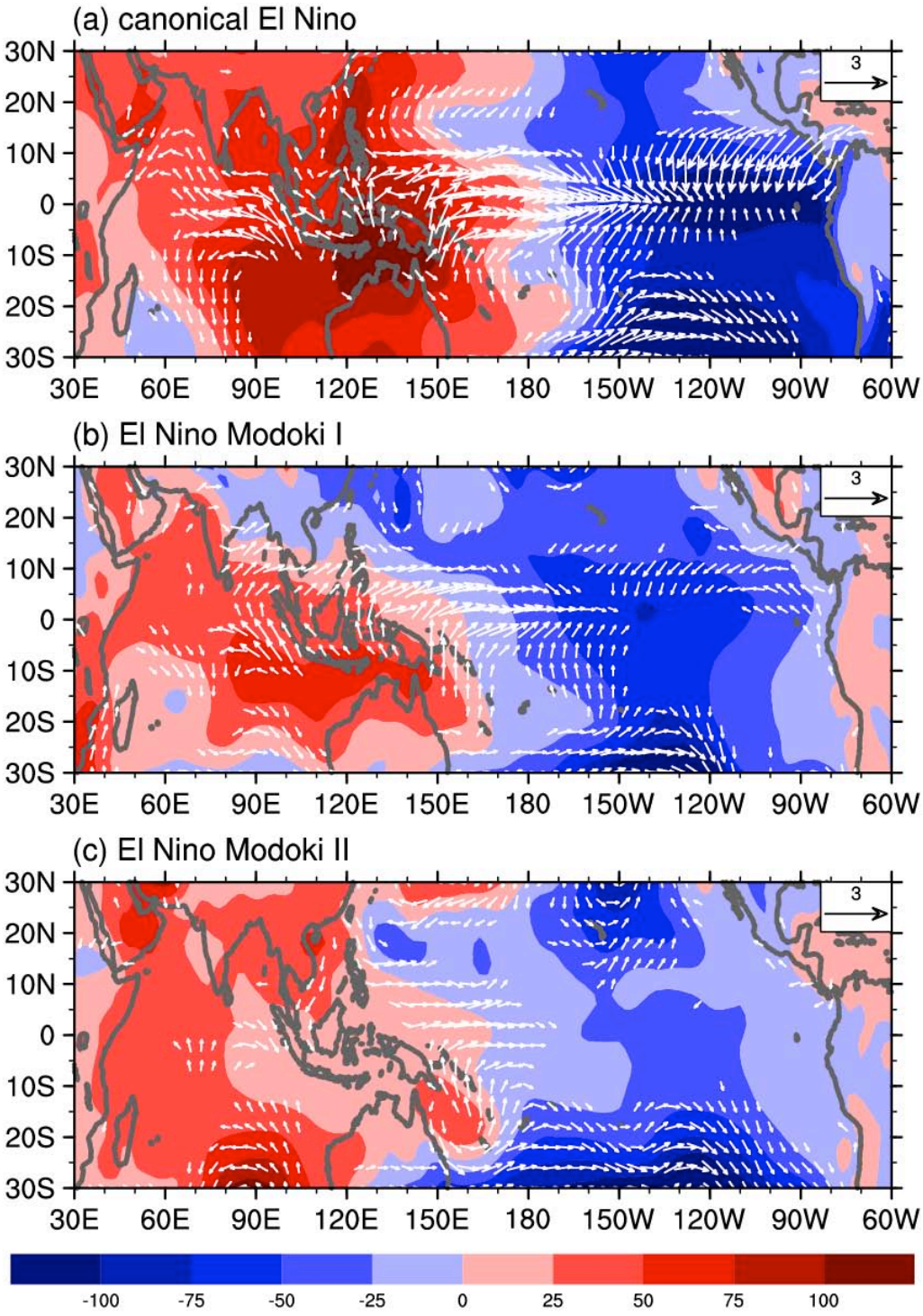

Figure 7. Composites of JASON-mean 1000-hPa wind (vector, m/s) and SLP (shading, Pa) anomalies for different types of El Niño. Shown are for (a) canonical El Niño, (b) El Niño Modoki I and (c) El Niño Modoki II. Only the wind anomalies exceeding 0.4 m/s are plotted.

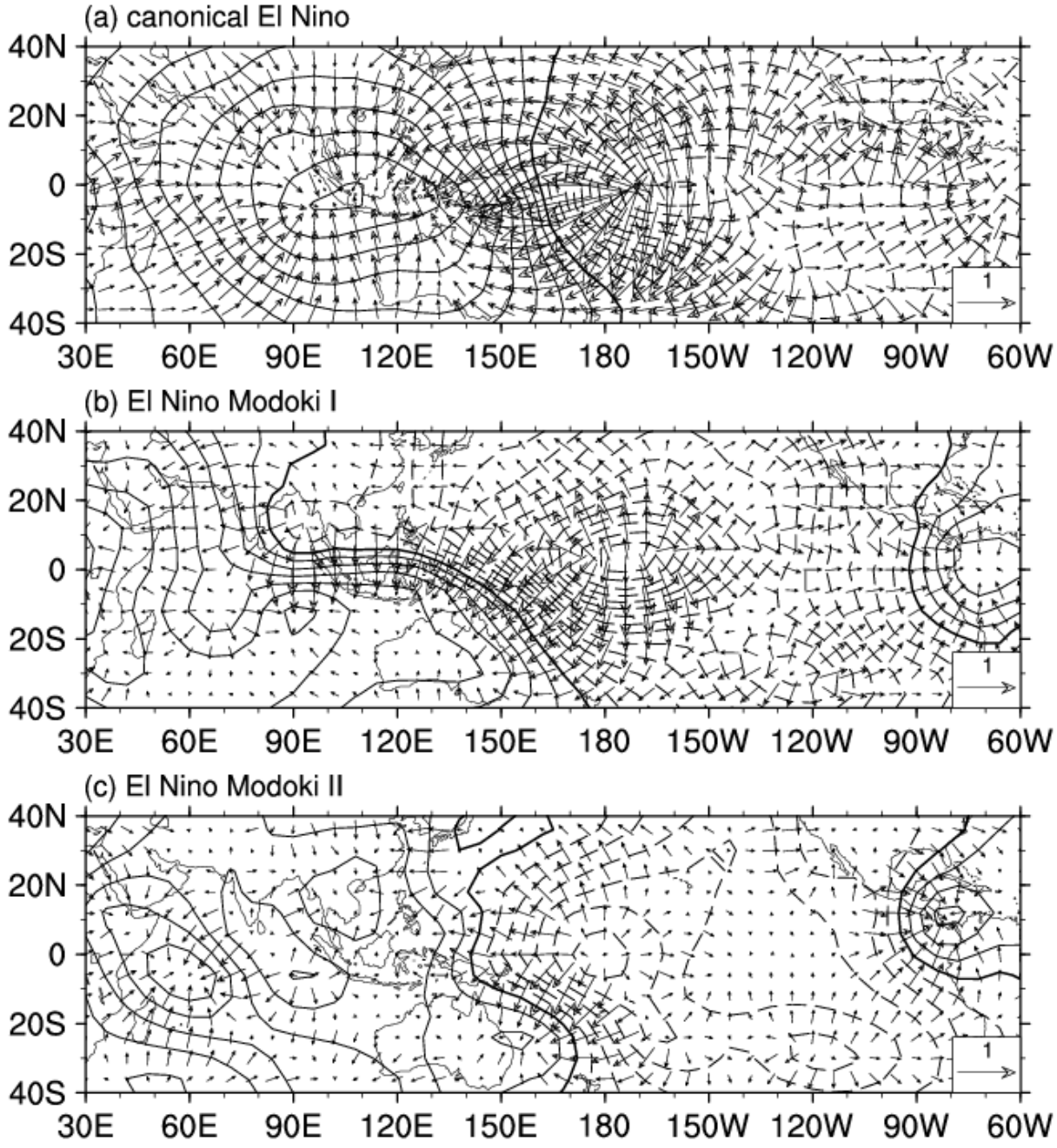

Figure 8. Composites of JASON-mean 200-hPa velocity potential (contour, 10^6 m^2 s^{-1}) and divergent wind (vector, m/s) anomalies for different types of El Niño. The zero contour line is thickened, and contour interval is 0.2 $\times 10^6$ m^2 s^{-1}. Shown are for (a) canonical El Niño, (b) El Niño Modoki I and (c) El Niño Modoki II.

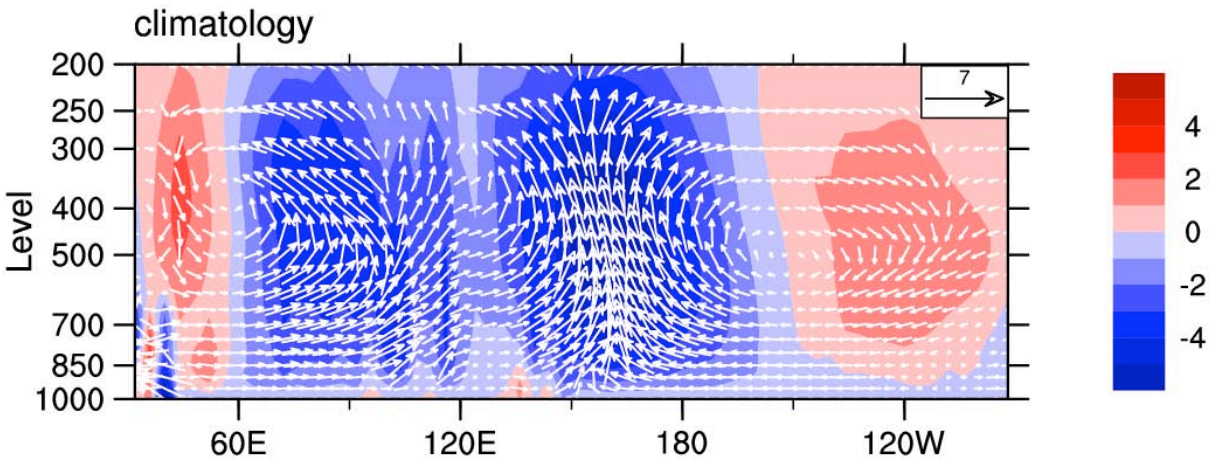

Figure 9. The JASON-mean climatology of zonal-vertical circulation by averaging zonal component of divergent wind and vertical velocity (scaled by -100) between 10°S and 10°N. Shadings are pressure vertical velocity anomalies scaled by 100.

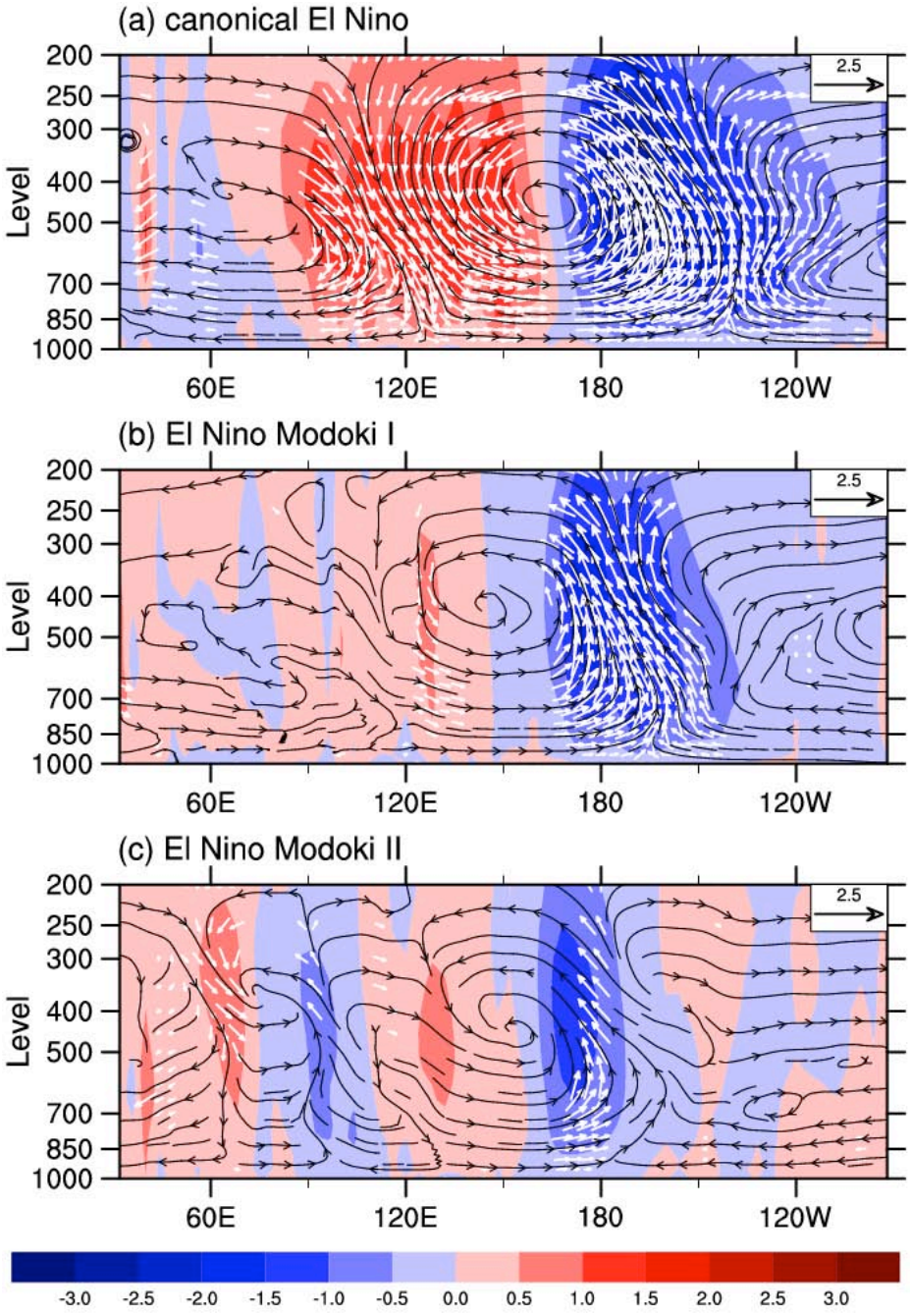

Figure 10. The streamline composites of JASON-mean zonal-vertical circulation anomalies by averaging zonal component of divergent wind and vertical velocity (scaled by -100) between 10°S and 10°N for different types of El Niño. Shown are for (a) canonical El Niño, (b) El Niño Modoki I and (c) El Niño Modoki II. The vectors indicate pressure vertical velocity exceeding 90% significant level based on Student's *t* test. Shadings are pressure vertical velocity anomalies scaled by 100.

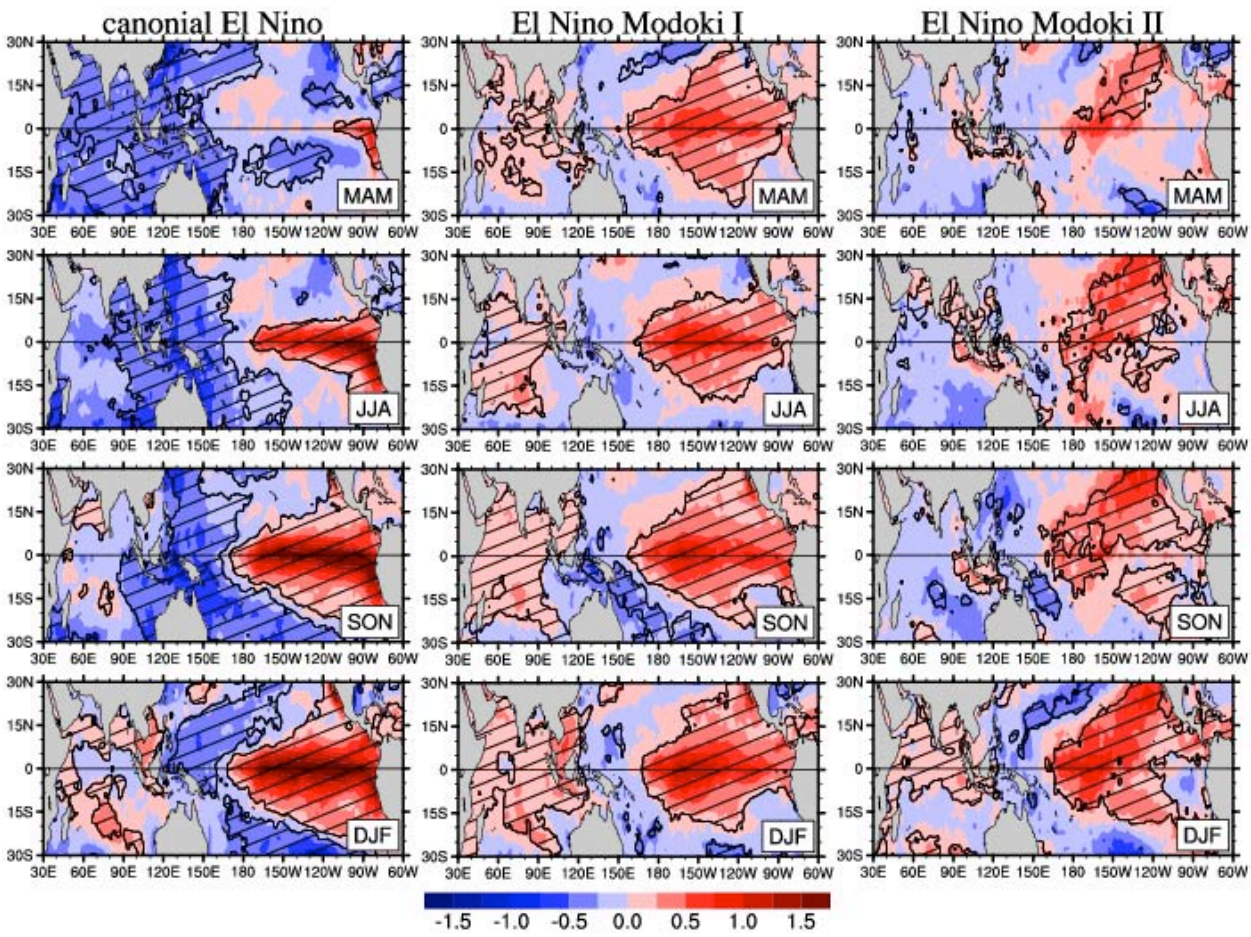

Figure 11. Same as Fig. 2 except for using the longer-term data from 1910-2008. The composites are calculated from eleven canonical El Niño events (1911/12, 1918/1919, 1925/1926, 1930/1931, 1951/52, 1957/1958, 1965/66, 1972/73, 1976/77, 1982/83, and 1997/98), eight El Niño Modoki I events (1914/15, 1940/41, 1941/42, 1963/1964, 1987/88, 1990/91, 1991/1992, and 2002/03), and five El Niño Modoki II events (1958/1959, 1968/69, 1979/80, 1992/93, and 2004/05).